

# Kinetic investigations of the laser-induced photolysis of sodium rhodizonate in aqueous solutions

H. Bettermann\*, I. Dasting<sup>1</sup>, U. Wolff

*Institut für Physikalische Chemie und Elektrochemie, Geb. 26.43, Heinrich-Heine-Universität Düsseldorf, Universitätsstr.1, 40225 Düsseldorf, Germany*

Received 4 March 1996; accepted 4 June 1996

## Abstract

The laser-induced photolysis of rhodizonate and tetrahydroxy-*p*-benzoquinone(4<sup>-</sup>) (THQ(4<sup>-</sup>)) has been studied with particular consideration of the photoreactions in de-aerated solutions. Both rhodizonate and THQ(4<sup>-</sup>) can be converted to croconate. The quantum yields using rhodizonate as the initial compound are very small ( $< 10^{-4}$ ) and depend on the applied irradiation technique. Compared with that finding, the photooxidation of rhodizonate in aerated solutions exhibits large quantum yields ( $\approx 0.05$ ) which are independent of the excitation wavelength and of the laser power. By increasing the local photon density in the irradiation of de-aerated solutions, a hitherto unknown photoproduct could be detected and was identified as the ring-enlarged species  $C_7O_7^{2-}$ . The seven-membered ring compound was characterized by UV/visible and Raman transitions in combination with theoretical investigations concerning the structure and vibrations of oxocarbons. This new aromatic oxocarbon decays with a half-life of about 20 min. Additionally, the alkaline hydrolysis of rhodizonate was reinvestigated at various temperatures. At room temperature the uniform reaction yielding THQ(4<sup>-</sup>) was quantified by the first order rate constant. At higher temperatures the quinone represents the only intermediate during the formation of croconate. This consecutive reaction was found to be independent of the presence of oxidizing agents. Therefore, the rearrangement mechanism suggested previously has to be revised. © 1997 Elsevier Science B.V. All rights reserved.

**Keywords:** Kinetic analysis; Laser photolysis; Oxocarbon; Quantum yield; UV/visible spectroscopy

## 1. Introduction

The oxocarbons represent a class of compounds with the general formula  $C_nO_n^{q-}$ . The experimentally well-known species are those with

$n = 3-6$  and  $q = 0, -2$  (for  $n = 6$  also  $q = -4, -6$ ). The spectroscopically most interesting compounds  $C_nO_n^{2-}$  have symmetrical structures with  $D_{nh}$  geometry. They derive their aromatic character from the cyclically delocalized  $\pi$ -bonds and exhibit unusually high stability [1]. Besides these oxocarbons, the reduced form of the rhodizonate, the tetrahydroxy-1,4-benzoquinone tetraanion (THQ(4<sup>-</sup>)), is of major importance, as the redox

\* Corresponding author; e-mail: betterma@clio.rz.uni-duesseldorf.de

<sup>1</sup> Forms part of this author's thesis.

system triquinoyl/rhodizonate/THQ(4<sup>-</sup>) is involved in the degradation of DNA [2]. Fig. 1 depicts the relevant oxocarbons discussed in our contribution. It has long been known that aromatic oxocarbons undergo photochemical decomposition that depends strongly on the presence of electron acceptors (dissolved oxygen in particular) in their solutions. The same is true for the alkali-induced conversion of rhodizonate to croconate, which was described as a quantitative method in 1975 [3], but no systematic study of this fruitful research field was presented until the investigations of Iraci and Back [4] were published.

The photochemistry of oxocarbons is of interest from three main viewpoints. First, it is still an open question whether the photochemical processes are similar to those of aromatic or polycarbonyl compounds. Second, the possible application of rhodizonate for the conversion of solar energy into photoelectrochemical energy depends directly on its photostability. Third, rhodizonate and more especially croconate are known to serve as photoinitiators for radical polymerisation [5]. For the first consideration in particular, THQ(4<sup>-</sup>) also plays an important role because this anion links the photochemistry of oxocarbons and quinonoid compounds. The latter show various types of photoreactions on excitation of the bathochromic  $\pi-\pi^*$  or  $n-\pi^*$  transition. Previous investigations for *o*-chloranil showed photodimerisation in CCl<sub>4</sub> and photoaddition to benzene [6]. 3,5-Di-*t*-butyl-1,2-benzoquinone exhibited CO elimination on exciting the  $\pi-\pi^*$  transition with a preceding bisketene intermediate [7], whereas photodimerisation occurs on exciting the  $^1n-\pi^*$  transition [8].

The investigations of Iraci, Zhao and Back [4,9] were restricted to the photo-reactions of rhodizonate with oxygen in aerated solutions and with other inorganic [Fe(CN)<sub>6</sub><sup>3-</sup> or H<sub>2</sub>O<sub>2</sub>] or organic electron acceptors (e.g., tetracyanoethylene). In contrast, the irradiation of de-aerated solutions was found to be inefficient, both with cw irradiation [10] and on flashlith photolysis [11].

In our contribution, we present the photochemical behaviour of rhodizonate and THQ(4<sup>-</sup>) on the excitation of their lowest  $^1\pi-\pi^*$  transition with an argon ion laser at different output powers

in the range between 10<sup>16</sup> and 10<sup>17</sup> quanta cm<sup>-2</sup> s<sup>-1</sup>, i.e. two orders of magnitude larger than the light intensities mentioned in [10] or [11]. The photokinetic investigations were carried out with both aerated and de-aerated solutions in order to determine the integral quantum yields and to identify the reaction pathways of oxocarbons by the detection of photoproducts in particular. Additionally, the thermal reaction of rhodizonate in alkaline buffered solutions was reinvestigated with respect to the determination of the rate constant and to the influence of temperature or oxygen content. In this context, the previously suggested mechanism for the conversion of rhodizonate to croconate basing on the  $\alpha$ -oxo-alcohol rearrangement (benzilic acid type, cf. [12]) has to be checked.

## 2. Experimental

### 2.1. Sample preparation

Sodium rhodizonate (Merck, > 98.5%) was used without further purification. The oxocarbon was dissolved in water (Merck, chromatography label, > 99.9995%) for the photochemical investigations and in a buffer solvent at pH = 11 (Fa. Kraft, glycol/NaCl/NaOH) for the hydrolysis reaction. THQ(4<sup>-</sup>) was prepared by dissolving sodium rhodizonate in 1 N NaOH at room temperature. The solutions were thoroughly flushed with nitrogen over a purging period of 30 min in a cell constructed for this purpose, except for the photooxidation reactions. The solutions were then transferred to the UV/vis block cell or the Raman cell, contact with atmospheric oxygen being excluded by a nitrogen flow.

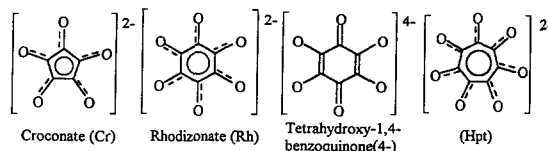


Fig. 1. The investigated oxocarbons; Hpt is 6,7-dihydroxy-6-cycloheptene-1,2,3,4,5-pentaone(2<sup>-</sup>).

## 2.2. Photolysis monitored by UV/vis spectroscopy

The UV/vis absorption spectra were recorded with a diode-array spectrometer (HP 8452 A) in the range 200–650 nm. The cycle time for the measurements on aerated solutions of rhodizonate was 1 s at an integration time of 0.2 s and that for de-aerated solutions was 60 s at an integration time of 2 s. The resolution for all reaction spectra was 2 nm. Recordings were computer-controlled using HP 89531A software, which additionally provides the analysis and fit of zero-order and first-order kinetics.

The photochemical reactions were induced in a block cell (Hellma, 119.000F-QS) with four transparent windows (1 cm path length) using the single emission lines at 457.9, 476.5, 488.0, 496.5 and 514.5 nm of an Ar<sup>+</sup> laser (Spectra-Physics, model 2030). The laser beam was propagated perpendicularly to the optical axis of the spectrometer. The temperature of the cell was stabilized at 298 K by a thermostat (Haake F). For extensive illumination of the sample, covering about 35% of the total area of the entrance window, the laser beam was expanded by a cylindrical lens placed 20 cm in front of the entrance window. For irradiation at the highest photon density, the laser beam was focused into the cell by a convex lens with a focal length of 40 cm. In this case, the solutions must be absolutely free from dust particles, as otherwise particles would be deposited and decomposed at the entrance window. Furthermore, the solutions were stirred during the measurements in order to avoid concentration and density gradients within the cell. These could occur owing to local heating on irradiation with the focused laser beam in particular. For the quantitative determination of reaction rates and the construction of the absorbance-difference plots, the paired absorbance–time values were converted so that the required routines of the program KINETIK [13] could be used.

## 2.3. Photolysis monitored by resonance Raman spectroscopy

The Raman spectra were detected by a grating spectrometer (Jarrell-Ash 25-400 Czerny–Turner

type double monochromator, 1 m focal length) and a Peltier-cooled photomultiplier (RCA C31034) with a subsequent photon counting system. The Ar<sup>+</sup> ion laser transition at 514.5 nm was used to generate the resonance Raman spectrum in the spectral range 300–600 cm<sup>-1</sup> (Stokes shift). The excitation power of the laser was set to 500 mW. The fixed slit width setting of the monochromator (entrance/intermediate/exit slit: 1200/300/600 μm) provides a spectral resolution of 9 cm<sup>-1</sup> at 488.0 nm. The scan speed of the monochromator was set to 100 cm<sup>-1</sup> min<sup>-1</sup> with a step width of 0.5 cm<sup>-1</sup>. The scattered light was collected at right angles to the excitation laser beam. The signal processing included smoothing by Fourier filtering [14] and removal of background fluorescence.

For the preparation of photoproducts, the sample was irradiated at 457.9 nm over periods of 20 min with a focused laser beam, which was directed into the stationary cylindrical Raman cell (see the discussion in Section 4.5). The Raman spectra were then recorded using the same cell, but now rotating in order to avoid local heating inside the liquid sample and to prevent further photochemical decay [15]. These alternating steps were repeated until the Raman signals of the photoproduct attained their highest intensity.

## 3. Methods

### 3.1. Determination of integral quantum yields

The determination is carried out according to the procedure described in [19]. The photochemically induced decrease of a species A (in this case the initial compound rhodizonate, abbreviated as Rh) for a simple primary step of a photoreaction  $A \xrightarrow{h\nu} B$  can be written as follows

$$\frac{d[\text{Rh}]}{dt} = -1000I_0F(A')\Phi_r\varepsilon'_{\text{Rh}}[\text{Rh}] \quad (1)$$

where  $F(A')$  denotes the so-called photokinetic factor with

$$F(A') = \frac{1 - 10^{-A'}}{A'} \quad (2)$$

and includes the time-dependent absorbance at the excitation wavelength  $\lambda'$ . It should be noted that all primed quantities are related to the excitation wavelength. The factor 1000 fits the volume unit (litres to  $\text{cm}^3$ ) on both sides of Eq. (1). The integration of Eq. (1) leads to

$$\Phi = \frac{\Delta c d}{v_i \cdot 1000 \cdot I_0 \int_0^t 1 - 10^{-A'(t)} dt} \quad (3)$$

where  $v_i$  denotes the stoichiometric factor for the initial step (usually  $v_i = 1$ ),  $I_0$  is the light intensity,  $d$  is the absorption path length and  $\Delta c = ([\text{Rh}]_0 - [\text{Rh}]_t)$  denotes the conversion of the initial compound. The decisive quantity in Eq. (3) is that part of time during the whole irradiation period under consideration during which the laser light was totally absorbed.

This is expressed by the integral, the type of which depends on the time law used for the fit of  $A'(t)$ . A zero-order fit requires the evaluation of the following integral

$$\int_0^t (1 - 10^{-A'(t)}) dt = t \left|_0^t - \frac{1}{\ln 10 m'} 10^z \right|_{z(0)}^{z(t)} \quad (4)$$

where the substitution variable  $z(t)$  corresponds to

$$z(t) = -A'_0 + m't \quad (5)$$

The only fit parameter is the rate constant  $m'$ , which has to be optimized to achieve a minimum standard deviation for  $A'(t)$  over as long a time range as possible. Because of the higher accuracy, this quantity was not directly evaluated for the excitation wavelength, but was derived from the analysis wavelength with respect to the different absorbances.

Applying the same procedure for a first order time law, only the integral in Eq. (3) must be replaced. As the integral type  $\int 10^{-a \cdot \exp(-bt)} dt$  cannot be directly solved, the expression was calculated using a series formula

$$\int_0^t 1 - 10^{-A'(t)} dt = t \left|_0^t + \frac{1}{k} \left( \ln |z| + z + \frac{z^2}{2 \cdot 2!} + \frac{z^3}{3 \cdot 3!} + \dots + \frac{z^n}{n \cdot n!} \right) \right|_{z(0)}^{z(t)} \quad (6)$$

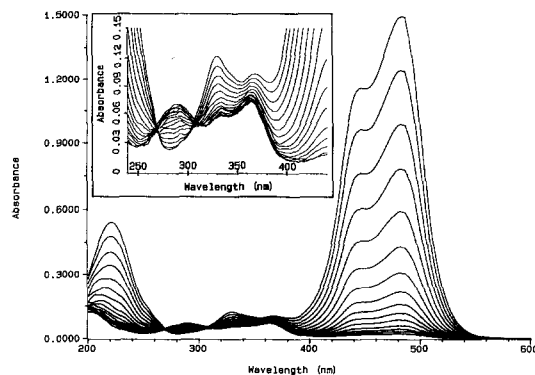


Fig. 2. Photoreaction spectrum of the aerated solution using an expanded laser beam ( $\lambda' = 496.5$  nm, 45 mW);  $\Delta t = 4$  s. Inset: enlarged wavelength range of the photoproduct absorption.

with the substitution

$$z(t) = -\ln 10 A'_0 \cdot e^{-kt} \quad (7)$$

The polynomial terms were taken into account up to  $n = 10$  to achieve convergence. The fit parameter  $k$  denotes the first order rate constant according to the above mentioned criteria, assuming that the infinity value of  $A'(\infty) = 0$ .

The light intensity  $I_0$  appearing in the denominator of Eq. (3) was measured with a calibrated power meter (Coherent, model 212). This direct method is necessary because a suitable actinometer system for the high  $\text{Ar}^+$  laser intensities in the blue-green wavelength range has not yet been developed. The measured values must be related to the total irradiated area of the cell (about  $4 \text{ cm}^2$  for the block cuvette used) and to the specific molar photon energy.

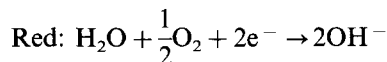
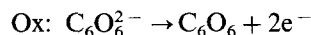
## 4. Results and discussion

### 4.1. Photolysis of rhodizonate in aerated solutions

The marked decomposition of rhodizonate in aqueous solution is caused by rapid photooxidation. Fig. 2 depicts the reaction spectra on irradiation with the laser line at  $\lambda' = 496.5$  nm and a moderate laser power of  $P_\lambda = 45$  mW. The rapid decrease of the allowed  ${}^1(\pi-\pi^*)$  absorption bands at 482 and 220 nm ( $A_{1g} \rightarrow E_{1u}$ ) corresponds to a

half-life of about 15 s. Additionally, a small increase of a transition at 288 nm, shown on an enlarged scale in the inset, and the decrease of the forbidden  ${}^1(\pi-\pi^*)$  transition ( $E_{2g}$  symmetry) at 328 nm of rhodizonate can be observed. The alterations within the range of small absorbances ( $A < 0.1$ ) are based on the short integration time of 0.2 s. The spectra intersect at 270 nm and over a narrow range at 304–308 nm. Although the very small absorbances of the only identified photoproduct prevent the formation of sharp isosbestic points (see Section 4.2), a uniform reaction can be assumed.

The spectroscopic data do not allow an unambiguous assignment. However, in accordance with [16,4] and our theoretical investigations concerning the evaluation of structures and vibrations of oxocarbons [17], the only possible product of the photooxidation is cyclohexanehexaone (triquinoyl), usually formed as the octahydrate [18]. The oxidation–reduction cycle corresponds to



where the generated hydroxide ions make the pH value increase only slightly because of the low initial concentrations.

A comparison of these results with those for croconate in [10] reveals the completely different behaviour on irradiation in spite of the close structural relationship and other common properties. The species cyclopentanepentaone (pentahydrate) cannot be detected, whereas the ring contraction of croconate to squarate is favoured even in the presence of oxygen. As indicated by the small absorption at 364 nm in Fig. 2, the latter pathway also occurs on the irradiation of rhodizonate, but the yield of croconate amounts to only about 5%.

The necessary quantities for the evaluation of the quantum yields using Eq. (3) in combination with Eq. (4) are as follows. The concentration differences  $\Delta c$  are in the range of  $(1-1.5) \times 10^{-5}$  M with  $c_0 \approx (3-4) \times 10^{-5}$  M. The laser power

of 45 mW, corrected for the reflection losses on all optical elements, corresponds to  $I_0 = 4.59 \times 10^{-8}$  mol  $\text{cm}^{-2}$   $\text{s}^{-1}$  ( $2.76 \times 10^{16}$  quanta  $\text{cm}^{-2}$   $\text{s}^{-1}$ ) at 488.0 nm. The integrated time for the total absorption period according to Eq. (4) amounts to 6–10 s, during which about 40% of the rhodizonate is converted.

The calculated quantum yields  $\Phi_1$  are listed in the first column of Table 1. First of all, it has to be pointed out that these values coincide well with those published in [4]. This is valid, although the light intensity given in [4] amounts to only 0.25 mW. This value is more than two orders of magnitude lower than for our experiment. Hence the quantum yields are obviously independent of both the light intensity and the excitation wavelength within the bathochromic  ${}^1\pi-\pi^*$  transition. Additionally, the oxygen content has no influence if the solution contains an excess of oxygen. Our aerated solutions were not purged, so that a maximum oxygen concentration of  $3 \times 10^{-3}$  M is present. This concentration exceeds that of rhodizonate by two orders of magnitude, whereas Iraci and Back used equivalent concentrations of both reactants.

#### 4.2. Photolysis of rhodizonate in de-aerated solutions

For all applications mentioned in the introduction (Section 1), the stability of rhodizonate solutions is a critical precondition. As shown in

Table 1  
Quantum yields of the photochemical reactions of rhodizonate: expanded laser beam propagation<sup>a</sup> and focused laser beam propagation<sup>b</sup>

$\lambda'/\text{nm}$	$\Phi_1^a$	$\Phi_2^a$	$\Phi_3^b$
457.9	0.050	$1.30 \times 10^{-4}$	$1.23 \times 10^{-4}$
476.5	0.046	$0.46 \times 10^{-4}$	$1.00 \times 10^{-4}$
488.0	0.044	$0.43 \times 10^{-4}$	$0.94 \times 10^{-4}$
496.5	0.044	$0.24 \times 10^{-4}$	$1.01 \times 10^{-4}$
514.5	0.043	$0.21 \times 10^{-4}$	$1.11 \times 10^{-4}$

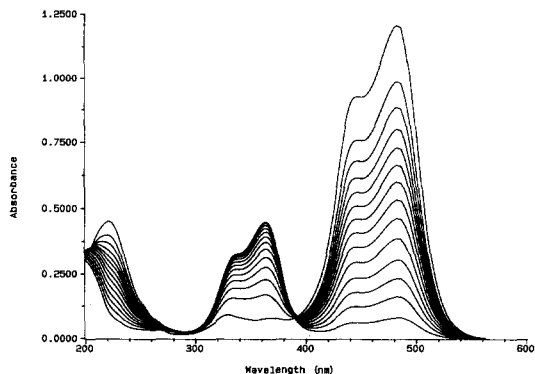


Fig. 3. Photoreaction spectrum of the de-aerated solution using an expanded laser beam ( $\lambda' = 488.0$  nm, 450 mW);  $\Delta t = 180$  s.

Section 4.1, rhodizonate undergoes an extremely rapid, irreversible photooxidation in the presence of oxygen. After thoroughly purging the solutions with nitrogen, photochemical decay or transient absorptions could not be detected either on laser irradiation during the recording of resonance Raman spectra [20] or on flashlight photolysis [11]. In contrast, we observed a slight bleaching of de-aerated solutions over longer irradiation periods during our resonance Raman measurements. A systematic kinetic study of this photoreaction with respect to the kinetics and to the determination of the quantum yield was therefore carried out.

Fig. 3 depicts the reaction spectrum on uniform irradiation of the cell. Croconate is the only identified photoproduct, characterized by its absorption feature with the maximum of the  $\pi-\pi^*$  transition ( $A'_1 \rightarrow E'_1$ ) at 364 nm. The yield of  $C_5O_5^{2-}$  amounts to about 40%, calculated from a molar absorptivity of  $\epsilon_{364} = 34\,000$  l mol $^{-1}$  cm $^{-1}$ ). The spectra intersect within the wavelength range 280–390 nm, where isobestic points do not appear. The uniformity of this reaction can be checked by correlating the decreasing absorbance (or absorbance differences) of the initial compound with the increasing absorbance of the appearing photoproduct for a series of reaction times. Linear relationships then establish uniformity, whereas non-linear relationships reveal the existence of intermediates [19]. In this case, the

corresponding wavelengths were selected as 220, 424, 448, and 482 nm for rhodizonate and 338 and 364 nm for croconate. The absorbance difference (AD) plot in Fig. 4 exhibits a single vertex with a small slope, so that only one intermediate at low concentration need be considered.

For this case the evaluation of the quantum yields requires a first-order analysis using Eq. (3) in combination with Eq. (6). The critical quantities are quite different from those of the photooxidation. The concentration differences  $\Delta c$  are in the range  $(0.5-1.2) \times 10^{-5}$  M with the same initial concentrations as in Section 4.1. The laser power of 450 mW corresponds to  $I_0 = 4.59 \times 10^{-7}$  mol cm $^{-2}$  s $^{-1}$  ( $2.76 \times 10^{17}$  quanta cm $^{-2}$  s $^{-1}$ ) at 488.0 nm. The fitted first-order rate constants are in the range  $(0.5-1.7) \times 10^{-3}$  s $^{-1}$ . According to Eq. (6), the integrated time for the period of total absorption amounts to 200–700 s, during which about 35% of the rhodizonate is converted, i.e. two orders of magnitude higher than the time required for the photooxidation.

As can be seen from the second column in Table 1, the quantum yields are more than two orders of magnitude smaller than those obtained from the photooxidation, and depend on the excitation wavelengths. The wavelength dependence of  $\Phi_2$  indicates a multi-photon process wherein the absorption of the intermediate is increased in the range of the blue Ar $^+$  laser emission lines.

As shown below, the comparison of results from UV/vis and Raman spectra is of importance

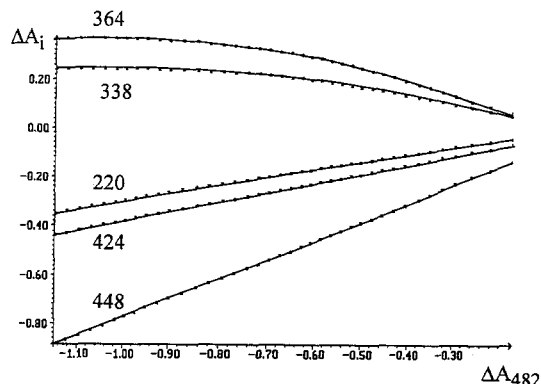


Fig. 4. Absorbance-difference plot relating to Fig. 3.

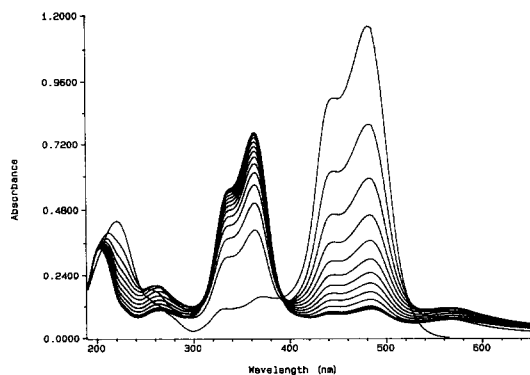


Fig. 5. Photoreaction spectrum of the de-aerated solution using a focused laser beam ( $\lambda' = 457.9$  nm, 450 mW);  $\Delta t = 180$  s.

for complete understanding of the photoreactions. As the local photon density is greatly increased during the recording of Raman spectra with a focused laser beam, the photokinetics were also investigated under this condition. Apart from the well known absorption profile of croconate, the reaction spectrum in Fig. 5 shows two additional transitions at 262 and 562 nm. These absorption bands appear immediately at the beginning of the irradiation, and they simultaneously reach maximum absorbance after about 10 min and decay synchronously. The red shift of the absorption band at 562 nm by about 80 nm ( $\approx 2000$   $\text{cm}^{-1}$ ) from that of the initial compound must be emphasized. This effect was never observed on laser irradiation of the carbonyl compounds first investigated. In contrast to the usual decomposing photoprocesses, a partial reaction step that provides an expansion of the framework must be taken into account. The identification of this unknown species is addressed in the discussion of Section 4.5.

Comparing the distribution of the photoproducts with that in the previously described photoreactions, the yield of croconate is substantially increased up to 60%. The AD plots (Fig. 6) relating to the wavelengths of the unknown photoproduct at 262 and 562 nm, those of croconate at 338 and 364 nm and those of rhodizonate at 256 and 482 nm proved the non-uniformity of the reactions. The vertices of each graph are much

more distinct than in the case of uniform illumination. Therefore a single intermediate has to be considered.

The evaluation of the quantum yields again requires first-order analysis using the following quantities. The concentration differences  $\Delta c$  are in the range  $(0.5-1.2) \times 10^{-5}$  M with the same initial concentration as above. Using the same laser power of 450 mW, the first-order rate constants are in the range  $(1-1.7) \times 10^{-3}$   $\text{s}^{-1}$ . In this case, the integrated time for the total absorption period varies between 200 and 400 s. The quantum yields (third column of Table 1), evaluated using a first-order fit for  $A'(t)$ , are independent of the excitation wavelengths. The values are constant within the range of experimental uncertainty with an average of  $\Phi_3 = 1.06 \times 10^{-4}$ . In addition, this independence indicates a different intermediate that does not absorb in the blue-green spectral range. The quantum yields  $\Phi_2$  and  $\Phi_3$  in the region of  $\leq 10^{-4}$  coincide well with the rough estimate in [10], where a quantum yield lower than  $10^{-3}$  was suggested (see Table 1).

#### 4.3. Photolysis of THQ(4-) in aerated solutions

As this reduced species of rhodizonate is of importance for the complete understanding of redox reactions of oxocarbons, the investigation of its photooxidation enables comparison with the photochemistry of croconate and rhodizonate. Because of the lower symmetry, the bathochromic  $\pi-\pi^*$  absorption of THQ(4-) splits into two

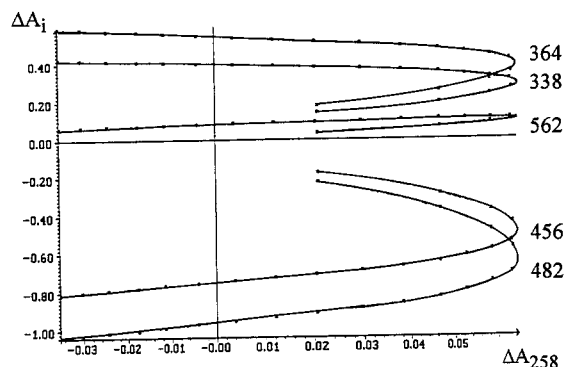


Fig. 6. Absorbance-difference plot relating to Fig. 5.

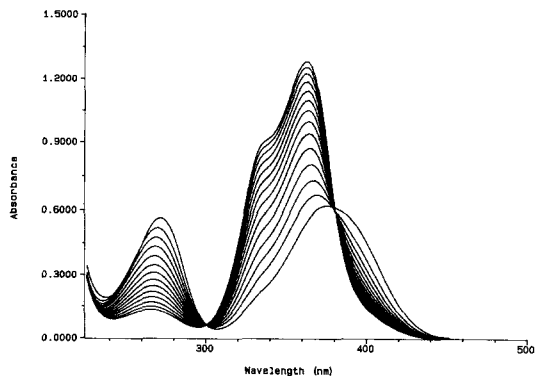


Fig. 7. Photoreaction spectrum of THQ(4<sup>-</sup>) at pH 14 ( $\lambda' = 457.9$  nm, 450 mW);  $\Delta t = 180$  s.

allowed transitions at 270 nm ( $A_g \rightarrow B_{1u}$ ) and 380 nm ( $A_g \rightarrow B_{2u}$ ). As the emission lines of an Ar<sup>+</sup> laser are less effective for the electronic excitation, the photoreaction of THQ(4<sup>-</sup>) could be induced only by the blue line at 457.9 nm. The reaction spectrum in Fig. 7 shows croconate as the only photoproduct. Distinct isosbestic points are visible at 300 and 380 nm. The assumption of a uniform photoreaction can be confirmed by linear absorbance-difference plots, e.g., analysing the wavelengths at 270, 286 and 402 nm for the initial compound in combination with those at 334 and 362 nm for the product. As the absorbances at 457.9 nm are very small, reliable values for  $A'(t)$  are not available, so that the procedure for the evaluation of quantum yields presented in Section 3 (Methods) could not be carried out. Nevertheless, a very high effectiveness of this photoreaction must be postulated, because a very few absorbed light quanta lead to nearly complete conversion.

The fact that croconate can be generated photochemically from both rhodizionate and THQ(4<sup>-</sup>) is in accordance with our structural investigations for the lowest excited state. Both semi-empirical (PM3 and AM1 method, for details see Section 4.5) and resonance Raman studies [17] reveal the structural coincidence of the S<sub>1</sub> states, i.e.  $D_{6h}$  symmetry for the  ${}^1E_{1u}$  state of rhodizionate and the  ${}^1B_{2u}$  state of THQ(4<sup>-</sup>), even though the C–O bond length is substantially increased in the case of THQ(4<sup>-</sup>). This is caused

mainly by the geometrical alteration within the *p*-quinonoid framework from  $D_{2h}$  to  $D_{6h}$ , whereas the structure of rhodizionate is only slightly altered in the S<sub>1</sub> state despite the Herzberg–Teller distortion.

#### 4.4. Thermal hydrolysis of rhodizionate at pH 11

The previously discussed photochemical reactions were carried out in weakly basic solutions at pH = 8.3. This corresponds to the actual basic strength of sodium rhodizionate. On dissolving rhodizionate in buffers at pH > 10, thermal conversion of rhodizionate to THQ(4<sup>-</sup>) takes place, and was reported for the first time in [4]. However, for this uniform reaction, the reaction order and the rate constants at various temperatures are still unknown. Therefore we reinvestigated the reaction from these aspects in a temperature range between 298 K ( $\vartheta = 25^\circ\text{C}$ ) and 313 K ( $\vartheta = 40^\circ\text{C}$ ) in steps of 3 K. Although a direct influence of dissolved oxygen on this thermal reaction could not be observed, all solutions were thoroughly purged with nitrogen to exclude any possible oxidative decay.

The reaction spectrum depicted in Fig. 8(a) has exactly the same features as described in [4] and exhibits uniform reaction as shown by the isosbestic points at 248, 304, 326, and 412 nm. The absorbance–time values can be fitted using a first-order time law for which a rate constant of  $k_1 = 2.0 \times 10^{-4} \text{ s}^{-1}$  is obtained by using the method of Swinbourne [13]. Assuming the complete conversion of rhodizionate to THQ(4<sup>-</sup>), the absorptivities for THQ(4<sup>-</sup>) are  $\epsilon(270) = 10\,700 \text{ l mol}^{-1} \text{ cm}^{-1}$  and  $\epsilon(380) = 11\,800 \text{ l mol}^{-1} \text{ cm}^{-1}$ . The absorption maxima are in the usual range for *p*-benzoquinones [21], whereas the very large values for the absorptivities, with  $\log \epsilon > 4$  point to the specific electronic properties of THQ(4<sup>-</sup>).

The investigations at higher temperature revealed a significant modification of the reaction spectrum. Fig. 8(b) shows an increase of the absorption profile of croconate accompanied by quasi-isosbestic points at 248 and 412 nm. The bathochromic absorption of THQ(4<sup>-</sup>) is now overlaid by the absorption of croconate. The hypsochromic band at 270 nm passes through a max-

imum after about 60 min, followed by a slight decrease. Based on these facts, the reaction mechanism can be described as a consecutive reaction:  $\text{Rh} \rightarrow \text{THQ}(4-) \rightarrow \text{Cr}$ . The non-uniformity of this thermal reaction is also confirmed by non-linear AD plots using the analysis wavelengths 272, 358 and 380 nm for the products in combination with those of rhodizionate at 456, 482 and 504 nm. The plot in Fig. 9 shows a single vertex for all combinations, so that only one intermediate, namely  $\text{THQ}(4-)$ , is involved in the formation of croconate.

These observations have two consequences. First, an evaluation of thermodynamic quantities with the use of the Arrhenius equation is not possible because of the dependence of the course of reaction on the temperature. Second, there are no spectral indications of the formation of intermediates suggested by the rearrangement mecha-

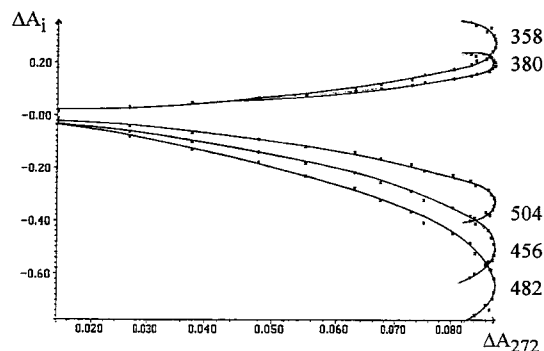


Fig. 9. Absorbance-difference plot relating to Fig. 8(b).

nism. At least the five-membered ring  $\alpha$ -hydroxycarboxylic acid should persist sufficiently for the detection of UV signals to be possible. Additionally, the rearrangement mechanism requires the presence of oxygen for the oxidative decomposition of the carboxylic group to  $\text{CO}_2$ . In contrast to this, we found that no kind of electron acceptor is necessary for the conversion but the capability for the oxidation of  $\text{THQ}(4-)$  is preserved in the first reaction step.

#### 4.5. Discussion of all reaction pathways

Finally, the previously introduced reactions can be now summarized in order to develop a complete reaction scheme. In this context, the most important aspects are the assignments of the UV/vis bands of the photoproducts and the mechanisms concerning the thermal conversion of rhodizionate to croconate and the ring-contraction or ring-enlargement reaction, respectively.

The red shift of the band at 562 nm (see Section 4.2) points to the fact that the delocalized  $\pi$ -system of the photoproduct is expanded. This band originates from the formation of the ring-enlarged aromatic oxocarbon  $\text{C}_7\text{O}_7^{2-}$ . This assumption is proved by additional experimental and theoretical data for Hpt. The special experimental investigations are based on resonance Raman spectra to locate the vibrational frequencies and on UV/vis spectra to monitor the thermal decomposition. The latter measurement is also essential for the determination of suitable conditions during the

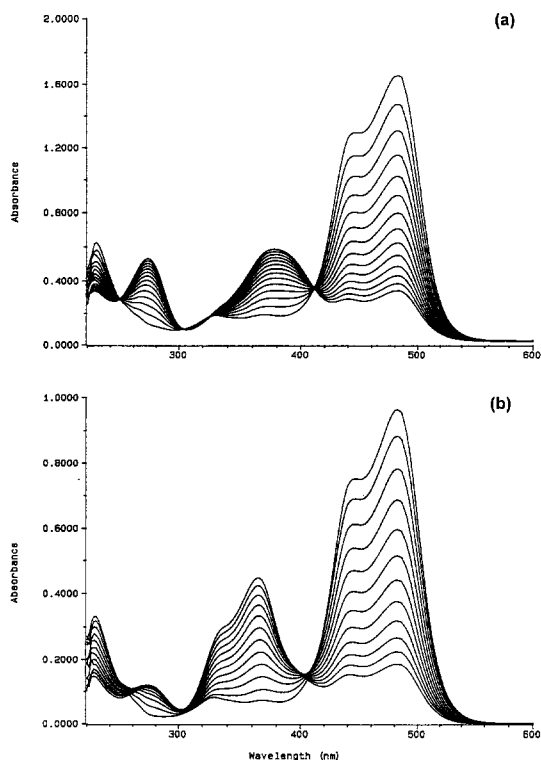


Fig. 8. Thermal reaction spectra in buffered solution at pH 11. (a)  $\vartheta = 25^\circ\text{C}$ ,  $\Delta t = 600$  s; (b)  $\vartheta = 40^\circ\text{C}$ ,  $\Delta t = 600$  s.

recording of resonance Raman spectra and for the correlation of absorption bands detected at 262 and 562 nm. The observation of the thermal decay was started after the induction period of 10 min, during which the maximum concentration was reached (cf. Fig. 5). Both absorptions decrease with the same first-order rate constant of  $6.5 \times 10^{-4} \text{ s}^{-1}$  and, as a result, the photoproduct has a half-life of 18 min. This result is supported by trajectory calculations concerning CO abstractions of oxocarbons [22] where  $\text{C}_7\text{O}_7^{2-}$  was predicted to be non-persistent.

Hence the recording times of the resonance Raman spectra must be restricted to a few minutes (see Section 2). Oxocarbons exhibit very characteristic Raman-active vibrations of A and E symmetry between 300 and 600  $\text{cm}^{-1}$ . The excitation wavelength at 514.5 nm provides a moderate resonance amplification both for Raman transitions of rhodizionate and for those of the photoproduct. This leads to enhanced sensitivity, which is necessary for the detection of Raman signals of  $\text{C}_7\text{O}_7^{2-}$  at very low concentration ( $\approx 10^{-6} \text{ M}$ ). The corrected Raman spectrum is depicted in Fig. 10.

Besides the transitions of rhodizionate at 432 and 553  $\text{cm}^{-1}$ , two additional bands at 449  $\text{cm}^{-1}$  and 494  $\text{cm}^{-1}$  appear. The latter normal modes correspond to the  $\text{E}'_2$  bending ( $D_{7h}$ ) and the totally symmetric breathing vibration, presented as insets in Fig. 10. The vibrational wavenumbers and

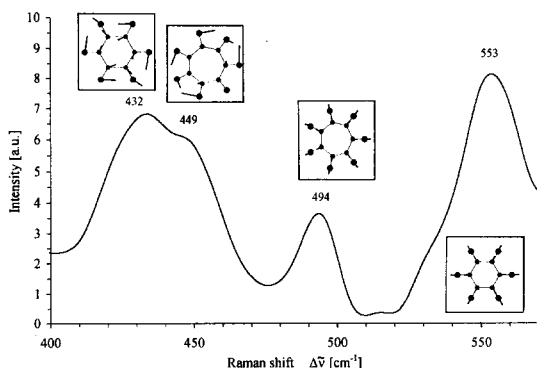


Fig. 10. Resonance-Raman spectrum of the de-aerated solution after irradiation with a focused laser beam;  $\lambda_0 = 514.5 \text{ nm}$  ( $\tilde{\nu}_0 = 19\,436 \text{ cm}^{-1}$ ), 500 mW. Insets: normal vibrations corresponding to the observed Raman transitions.

symmetries were confirmed by an ab initio optimized geometry for  $\text{C}_7\text{O}_7^{2-}$  obtained from the program GAUSSIAN92 [23] with a double-zeta basis set (HF/6-31G(d)) followed by a vibrational analysis. The GAUSSIAN92 calculations were performed with the tight SCF criterion, which is ten times lower than the default values, i.e.  $10^{-8}$  for the density gradient and  $10^{-5}$  for the energy gradient. In the case of Hpt the bond distances were calculated as  $r_{\text{C-C}} = 149.9 \text{ pm}$  and  $r_{\text{C-O}} = 121.3 \text{ pm}$  at a total HF energy of  $-788.91 \text{ H}$ . The optimization was carried out both with symmetry restriction ( $D_{7h}$ ) and with non-restricted geometrical parameters. For both cases the same geometry resulted, which is characterized by a highly symmetric planar structure. The very small torsions of the ring plane indicated by dihedral angles smaller than  $1^\circ$  can be disregarded. As shown from our calculations and previous structural investigations of the known aromatic oxocarbons in [22] and [26], the average deviation of the bond distances from the experimental values amounts to less than 2 pm using large double-zeta basis sets.

Using this theoretical approach for croconate and rhodizionate, constant scaling factors in the region of 0.9 were achieved [24]. Applying these factors to  $\text{C}_7\text{O}_7^{2-}$ , the vibrational frequencies were calculated as 457 ( $\pm 20 \text{ cm}^{-1}$ ;  $\text{E}'_2$  bending) and 477  $\text{cm}^{-1}$  ( $\pm 20 \text{ cm}^{-1}$ ;  $\text{A}'_1$  breathing) and coincide well with the above mentioned experimental data. The uncertainty of  $20 \text{ cm}^{-1}$  corresponds to the average deviation of about 5% (after scaling) derived from the comparison with the other oxocarbons squarate, croconate and rhodizionate. The accuracy is sufficient for our purposes, so that results from post-HF calculations (C.I., MP2, MP4) which could provide a further improvement of the vibrational frequencies (with a deviation as low as 2%) would not lead to other assignments.

A further simple check for the frequency of the breathing mode is its dependence on the ring size. In the case of aromatic oxocarbons the frequency decreases by 60–80  $\text{cm}^{-1}$  per additional CO unit (see Table 2). Moreover, it has to be stressed that the other possible photoproducts [croconate, squarate,  $\text{THQ}(4-)$ ] do not show any Raman-active transitions in the region of 500  $\text{cm}^{-1}$  (see Table 2).

Table 2

Structural, UV/vis and Raman data of aromatic oxocarbons  $C_nO_n^{2-}$ . Data for the non-aromatic THQ(4-)<sup>a</sup> and calculated data<sup>b</sup>

<i>n</i>	<i>r</i> <sub>C-C</sub> /pm	<sup>1</sup> π-π* (UV/vis)			A <sub>(1)g</sub> /A <sub>i</sub> (Raman)
		λ <sub>max</sub> /nm	$\tilde{\nu}_{max}$ /cm <sup>-1</sup>	Symmetry	Δ $\tilde{\nu}$ /cm <sup>-1</sup>
4	145.7	268	37300	<sup>1</sup> E <sub>u</sub>	723
5	145.7	364	27470	<sup>1</sup> E <sub>i</sub>	637
6	148.8	220	45450	<sup>1</sup> E <sub>1u</sub>	553
		482	20750		
7	149.9 <sup>b</sup>	262	38170	<sup>1</sup> E <sub>i</sub>	494
		562	17790		
6 <sup>a</sup>		272	36765	<sup>1</sup> B <sub>1u</sub>	601
		380	26315	<sup>1</sup> B <sub>2u</sub>	

The red shift of about 80 nm relative to the low-energy absorption of rhodizonate also indicates the formation of  $C_7O_7^{2-}$  if Platt's perimeter model is applied to this problem. This is known to be a very good qualitative description for the electronic transitions of both aromatic hydrocarbons and oxocarbons [25]. The correlation of the  $S_0$ - $S_1$  gap with  $1/u^2$  (*u* is the perimeter length,  $u = nr_{C-C}$ ) is linear for the experimental values of squarate, croconate and rhodizonate (see Table 2), as shown by the correlation coefficient of  $r = 0.9998$ . The extrapolation for the ring-enlarged species  $C_7O_7^{2-}$  leads to an electronic gap of about  $16\,500\text{ cm}^{-1}$  ( $\approx 600\text{ nm}$ ).

A semi-empirical geometry optimization (HF/PM3 and HF/AM1) of the  $S_1$  state for all aromatic oxocarbons  $C_nO_n^{2-}$  ( $n = 4-8$ ) [17,26] using the MOPAC 7.0 program [27] confirmed this gap size. All structural optimizations of the investigated oxocarbons for the  $S_0$  and the  $S_1$  state were carried out at a tight SCF limit ( $1 \times 10^{-6}\text{ kcal mol}^{-1}$ ) and a small geometry termination criterion (GNORM = 0.005). The energy gap was then calculated for the seven-membered ring compound as being  $17\,000\text{ cm}^{-1}$  (588 nm) with a correlation coefficient of  $r = 0.9995$ . Both correlations agree well with the experimental values of 562 nm for the maximum absorption and of  $\approx 620\text{ nm}$  for the range of the 0-0 transition, the spectral position of which can only be estimated. The PM3 method yields better coincidence of the observed with the calculated electronic gap than the formerly presented CNDO/S treatment [26]

(at least for the gap between the ground state and the bathochromic <sup>1</sup>E<sub>1u</sub> state). This is valid even though the  $S_1$  geometry using the default options of the keyword "excited" is based only on a C.I. calculation with few  $\pi$ -electrons in four orbitals. Thus, we estimate the error width for the electronic gap to be smaller than  $\pm 1000\text{ cm}^{-1}$  ( $\pm 30\text{ nm}$  at 588 nm).

An analogous treatment for the hypsochromic transition at 262 nm cannot be carried out because the corresponding absorptions of squarate and croconate are located in the vacuum-UV region and are therefore not readily observable. This electronic transition might be principally attributed to the <sup>1</sup>E<sub>u</sub> band of squarate. However, three arguments exclude this assumption. First, both absorptions (262 and 562 nm) must originate from one compound, since they decrease simultaneously (see above). Moreover, squarate is known to be a persistent compound in solution, and investigations reveal neither photochemical nor thermal decomposition (see [28,10]). In the latter reference, it is stated that squarate is obtained on the irradiation of croconate only in oxygen-containing solutions. This consecutive reaction step cannot occur under our chosen conditions.

The observed UV/vis and Raman signals identify the unknown photoproduct as the seven-membered ring compound  $C_7O_7^{2-}$ . This immediately raises the question as to the mechanism of the CO insertion. The established ring-enlargement mechanisms, e.g., those presented in [29], do not offer a reasonable explanation, as most reactions

include steps with incorporation of a side-chain. A similar thermal reaction is the insertion of carbene into benzene, which is assumed to be a *cis*-1,1-electrocyclic addition with a bicyclic intermediate [30]. Replacing carbene by CO and benzene by excited rhodizonate, an analogous course seems to be possible. The photoreaction was therefore also carried out with solutions thoroughly purged with carbon monoxide, but no increase in the yield of  $C_7O_7^{2-}$  could be detected. Another conceivable mechanism requires the formation of an excimer intermediate  $[Rh_2^*]$  with sandwich-type structure. The interaction leads to a ring-member exchange, which finally generates a ring-contracted species  $C_5O_5^{2-}$  and a ring-enlarged compound  $C_7O_7^{2-}$  via either a photochemical or a thermal pathway. This is in accordance with the higher yield of croconate if the other pathway (II, Fig. 12) continues to proceed simultaneously. The latter proposed mechanism is depicted in Fig. 11.

The quantum yield with respect to this mechanism depends on the concentration and the laser power. The formation of excimers is favoured at high concentration and high photon densities owing to multi-photon absorption processes. As suitable trapping reactions for this non-persistent photoproduct are still lacking, it is planned to support our results by further spectroscopic data. For example, a singlet  $^{13}C$  NMR signal in the region of  $\delta = 160$  ppm can be expected from a comparison with the data in [18].

All the investigated reaction pathways are summarized in Fig. 12. Path I describes the photooxidation with a quantum yield  $\Phi_1$ . It is surprising that a corresponding reaction for croconate is not known, but the ring-contracted compound squarate is generated in the presence of oxygen.

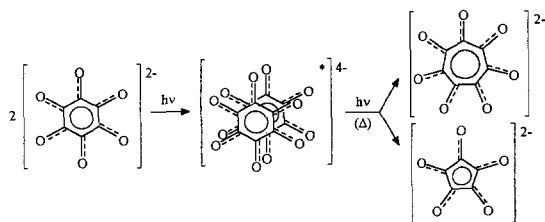


Fig. 11. Suggested mechanism for the formation of  $C_7O_7^{2-}$ .

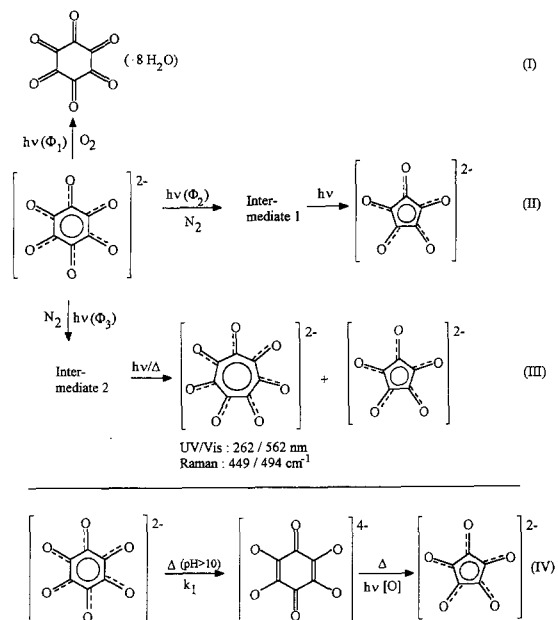


Fig. 12. Survey of all investigated reactions.

Just the opposite is true for irradiations of rhodizonate, in which the ring-contracted species croconate is obtained only under deoxygenated conditions (paths II and III). Path II describes the formation of croconate with uniform sample irradiation, and the photoreaction on irradiation with the focused laser beam is depicted in path III, as supplied by the decisive spectral data of  $C_7O_7^{2-}$ . As discussed in Section 4.2, two different intermediates must be taken into account because of the different wavelength dependence of  $\Phi_2$  and  $\Phi_3$ . In path IV, the thermal consecutive reaction is presented. In general, the thermal reaction, quantified at  $\vartheta = 25^\circ C$  with the rate constant  $k_1$ , is too fast to allow simultaneous observation of the concurrent photochemical decompositions, even in the case of aerated solutions.

## 5. Conclusions

- Rhodizonate in de-aerated solutions can be photochemically converted to croconate, even though the quantum yields are very small ( $\Phi \leq 10^{-4}$ ) compared with those of the reactions in aerated solution ( $\Phi \approx 0.045$ ). Hence the maxi-

mum yield for croconate of about 40–60% can be achieved only by laser irradiation. Croconate can also be prepared by the photooxidation of THQ(4–) at pH 14. This was proved to be a uniform reaction.

- A new oxocarbon compound was detected when the local photon density was drastically increased by focusing the Ar<sup>+</sup> laser beam. The photoproduct was identified as the ring-enlarged aromatic species C<sub>7</sub>O<sub>7</sub><sup>2-</sup> by very characteristic UV/visible and Raman transitions. The spectral data coincide well with experimental and theoretical data within the homologous series C<sub>n</sub>O<sub>n</sub><sup>2-</sup>.
- The investigation of the thermal conversion of rhodizonate to croconate at pH 11 and  $\vartheta = 40^{\circ}\text{C}$  revealed that the earlier suggested mechanism following the  $\alpha$ -oxo-alcohol rearrangement must be revised. On the one hand, the UV/vis reaction spectrum shows that THQ(4–) is the only observed intermediate and the intermediates suggested in [1,10] and [12] did not occur. On the other hand, an influence of oxygen that was postulated as being necessary for the conversion could not be found.

## References

- [1] R. West (Ed.), in Oxocarbons, Academic Press, New York, 1980, Ch. 1.
- [2] R. Schrebler, R. Araya, A. Arratia, D. Ciampi, M. Hoffman and N. Duran, *Bioelec. Bioenerg.*, 17 (1987) 523.
- [3] L.M. Schwartz, R.I. Gelb and Y.O. Yardley, *J. Phys. Chem.*, 79 (1975) 2246.
- [4] G. Iraci and M.H. Back, *Can. J. Chem.*, 66 (1988) 1293.
- [5] B. Zhao and M.H. Back, *J. Polym. Sci. A*, 30 (1992) 2399.
- [6] H. Bettermann and H.-J. Schroers, *Spectrochim. Acta Part A*, 47A (1991) 893.
- [7] B. Alkenings, H. Bettermann, I. Dasting and H.-J. Schroers, *Spectrochim. Acta Part A*, 49A (1993) 315.
- [8] V. Mostert, Diplomarbeit, University of Düsseldorf, 1995.
- [9] B. Zhao and M.H. Back, *Can. J. Chem.*, 69 (1991) 528.
- [10] B. Zhao and M.H. Back, *Can. J. Chem.*, 70 (1992) 135.
- [11] B. Zhao and M.H. Back, *Int. J. Chem. Kinet.*, 26 (1994) 25.
- [12] R. West, *Isr. J. Chem.*, 20 (1980) 300.
- [13] H.-H. Perkampus and R. Kaufmann, *Kinetische Analyse mit Hilfe der UV/VIS-Spektrometrie*, Verlag Chemie, Weinheim, 1991.
- [14] H. Bettermann and W. Rauch, *Appl. Spectrosc.*, 44 (1990) 1534.
- [15] W. Kiefer and H.J. Bernstein, *Appl. Spectrosc.*, 25 (1971) 500.
- [16] R.A. Chalmers and G.M. Telling, *Microchim. Acta*, 6 (1967) 1126.
- [17] H. Bettermann and I. Dasting, in preparation.
- [18] W. Städeli, R. Hollenstein and W. von Philipsborn, *Helv. Chim. Acta*, 60 (1977) 949.
- [19] H. Mauser, *Formale Kinetik*, Bertelsmann-Universitätsverlag, Düsseldorf, 1989.
- [20] M. Takahashi, K. Kaya and M. Ito, *Chem. Phys.*, 35 (1978) 293.
- [21] S. Berger, P. Hertl and A. Rieker, in S. Patai and Z. Rappoport (Eds.), *The Chemistry of Quinonoid Compounds*, Vol. II, Part 1, John Wiley & Sons, Chichester, 1988, Ch. 2.
- [22] L. Farnell, L. Radom and M.A. Vincent, *J. Mol. Struct.*, 76 (1981) 1.
- [23] GAUSSIAN 92, Revision D.1, M.J. Frisch, G.W. Trucks, M. Head-Gordon, P.M.W. Gill, M.W. Wong, J.B. Foresman, B.G. Johnson, H.B. Schlegel, M.A. Robb, E.S. Replogle, R. Gomperts, J.L. Andres, K. Raghavachari, J.S. Binkley, C. Gonzalez, R.L. Martin, D.J. Fox, D.J. Defrees, J. Baker, J.J.P. Stewart and J.A. Pople, Gaussian, Inc., Pittsburgh, PA, 1992.
- [24] P. Pulay, G. Fogarasi, G. Pongor, J.E. Boggs and A. Vargha, *J. Am. Chem. Soc.*, 105 (1983) 7037.
- [25] L.M. Schwartz, R.I. Gelb and D.A. Laufer, in R. West (Ed.), *Oxocarbons*, Academic Press, New York, 1980, Ch. 3.
- [26] C. Puebla and T. Ha, *J. Mol. Struct.*, 137 (1986) 171, 183.
- [27] J.J.P. Stewart, *MOPAC Program Package*, Version 7.0, QCPE No. 464, Austin, TX.
- [28] M. Iijima, Y. Udagawa, K. Kaya and M. Ito, *Chem. Phys.*, 9 (1975) 229.
- [29] M. Hesse, *Ring Enlargement Reactions in Organic Chemistry*, Verlag Chemie, Weinheim, 1993.
- [30] G.A. Russell and D.G. Hendry, *J. Org. Chem.*, 28 (1963) 1933.